

Magnetic properties and giant cryogenic magnetocaloric effect in *B*-site ordered antiferromagnetic $\text{Gd}_2\text{MgTiO}_6$ double perovskite oxide

Yikun Zhang^{a,b,c,*}, Yun Tian^b, Zhenqian Zhang^c, Youshun Jia^c, Bin Zhang^b, Minqiang Jiang^d, Jiang Wang^b, Zhongming Ren^b

^a School of Electronics and Information Engineering, Hangzhou Dianzi University, Hangzhou 310012, China

^b State Key Laboratory of Advanced Special Steels and Shanghai Key Laboratory of Advanced Ferrometallurgy and School of Materials Science and Engineering, Shanghai University, Shanghai 200444, China

^c Key Laboratory of Novel Materials for Sensor of Zhejiang Province, Hangzhou Dianzi University, Hangzhou 310012, China

^d State Key Laboratory of Nonlinear Mechanics, Institute of Mechanics, Chinese Academy of Sciences, Beijing 100190, China



ARTICLE INFO

Article history:

Received 2 August 2021

Revised 11 January 2022

Accepted 15 January 2022

Available online 17 January 2022

Keywords:

Magnetocaloric performances

Magnetic phase transition

Magnetocaloric (MC) effect

Rare earths based double perovskite oxides

ABSTRACT

The magnetic refrigeration (MR) technology by utilizing the magnetocaloric (MC) effects of magnetic solids have been realized to be a promising energy efficiency and environmentally friendly technology. Developing or discovering proper magnetic solids with promising MC performances is one of the most important tasks at present stage since a huge gap still exists between the requirement of practical MR application and the MC performances of the magnetic solids. Herein, we reported a combined theoretical and experimental investigation of the crystal structure together with the magnetic properties, magnetic phase transition (MPT) and MC performances in $\text{Gd}_2\text{MgTiO}_6$ oxide. The $\text{Gd}_2\text{MgTiO}_6$ is confirmed to crystallize in a *B*-site ordered monoclinic double perovskite (DP) crystal structure. A rather unstable antiferromagnetic (AFM) interaction with large magnetic moment and semi-conductor characteristic with the band gap of 2.977 eV have been confirmed in $\text{Gd}_2\text{TiMgO}_6$ DP oxide at ground state. Giant reversible cryogenic MC effect together with excellent MC performances have been confirmed by a series of the figure of merits including the values of maximum magnetic entropy change ($-\Delta S_M$) and refrigerant capacity (RC), which are evaluated to be 46.21 J/kgK and 300.27 J/kg around 3.3 K with the magnetic change of 0–7 T, these values are much better than most of the recently reported famous cryogenic MC materials and the commercialized magnetic refrigerants gadolinium gallium garnet (GGG) as well. The observed excellent MC performances suggest that $\text{Gd}_2\text{TiMgO}_6$ DP oxide is a promising candidate material for cryogenic MR applications.

© 2022 Acta Materialia Inc. Published by Elsevier Ltd. All rights reserved.

1. Introduction

The magnetic solids with both structural and magnetic phase transitions have attracted widespread attentions because of their unique and novel functional performances as well as potential applications in various advanced technologies [1–10]. Among those, the magnetic refrigeration (MR) method by utilizing the magnetocaloric (MC) effect of magnetic solids have been realized to be an attractive alternative technology to our current well-used gas compression/expansion technology [1–5]. The MC effect being an inherent magneto-thermodynamic phenomenon, manifests itself in the production and absorption of heat experienced by a magnet-

ically ordered material under the variation of external magnetic fields [1–3]. For this purpose, lots of studies have been dedicated for developing and discovering new materials exhibiting the appropriate MC effect at different working temperature regions from sub-Kelvin to the room temperature or above [11–22]. However, a huge gap still exists between the requirement of practical MR application and the MC performances of the magnetic solids. Developing and discovering proper magnetic solids with promising MC performances is one of the most important tasks at present stage.

The heavy rare earths (RE) based materials with highly localized 4f orbitals can be taken as good candidates for MC materials because of their large magnetic moments. Consequently, many selected RE based intermetallic compounds, oxides, amorphous alloys and molecular materials have been usually explored as potential magnetic refrigerants [23–33]. Several series RE-based intermetallics are reviewed very recently by Li and Yan in terms of the structure, magnetic phase transition (MPT) and MC perfor-

* Corresponding author at: State Key Laboratory of Advanced Special Steels and Shanghai Key Laboratory of Advanced Ferrometallurgy and School of Materials Science and Engineering, Shanghai University, Shanghai 200444, China.

E-mail address: ykzhang@shu.edu.cn (Y. Zhang).

mances [25]. Similarly, we have summarized the MPT, magnetic and MC performances in RE_2T_2X series intermetallic compounds recently [24]. Additionally, the RE -based oxides have received particular attentions due to the fact of easy to be fabricated as well as good physical and chemical stabilities, especially for the low cost of raw materials. Thus, large numbers of the RE -based oxides have been fabricated and determined systematically in terms of the MPT and MC effects as well. The RE -based double perovskite (DP) oxide with the general formula of $RE_2BB'_{\text{O}_6}$ (B and B' are two different transition metal elements) is as a sub-class of perovskite oxide have attracted special attentions due to their flexible combination of RE and B elementals [33,34]. Outstanding electrical, magnetic, optical, catalytic as well as MC properties have been reported by several research groups independently in $RE_2BB'_{\text{O}_6}$ DP oxides by suitable combination and selection of the RE and B atoms in recent years [33–40]. Considerable MC performances have been reported by us recently in $RE_2\text{CuMnO}_6$ [36] and $RE_2\text{FeAlO}_6$ [37] DP oxides. The investigation of magnetic properties and MC performances in $RE_2\text{ZnMnO}_6$ DP oxides with B site ordered structure [38] have illustrated that $\text{Gd}_2\text{ZnMnO}_6$ exhibits excellent MCE performances with $-\Delta S_M^{\max}$ of 25.2 J/kgK around 6.4 K under ΔH of 0–7 T [38]. Very recently, Xu et al. have fabricated $\text{Sr}_2\text{GdNbO}_6$ DP oxide and checked its magnetic properties and MC effect [39], pronounced $-\Delta S_M$ was realized with the peak value of 29.7 J/kgK around ~ 2 K. Very recently, the luminescence properties in the pure and doped $RE_2\text{MgTiO}_6$ DP oxides have been reported [40–42]. Whereas, the investigation on the magnetic and MC properties in $RE_2\text{MgTiO}_6$ DP oxides are still lacking. Herein we have further investigated the crystal structure, magnetic properties, MPT and MC performances of $\text{Gd}_2\text{MgTiO}_6$ DP oxide with aim to enlarge and deepen our understanding the fundamental mechanisms behind some of the DP oxides foundational performances and to figure out whether $\text{Gd}_2\text{MgTiO}_6$ is suitable for application in cryogenic MR application. Our findings illustrate that the studied $\text{Gd}_2\text{MgTiO}_6$ possesses a remarkably cryogenic giant MCE, which could be a promising candidate material for cryogenic MR applications.

2. Experimental and simulation details

The polycrystalline $\text{Gd}_2\text{MgTiO}_6$ oxide was synthesized by the transitional ceramic sol-gel route. Firstly, stoichiometric weight amount of $\text{Gd}(\text{NO}_3)_3$, $\text{Mg}(\text{NO}_3)_2$ and $\text{Ti}(\text{SO}_4)_2$ with the minimum purity better than 99.99% were completely dissolved into the deionized H_2O at ambient. Then, the citric acid (CA) was adjusted with the molar ratio of 2:1 for (CA):(Gd^{3+} + Mg^{2+} + Ti^{3+}). After that, the solution was evaporated by continuous stirring at 355 K to obtain an organic resin that includes a homogeneous distribution of all the cations, consequently the resin was directly dried at 373 K for 12 h in air. Later on, the resulting dried gel was grounded and fired at 800 K for 5 h to eliminate all the organic residues, sulfates and nitrates. Finally, the well-prepared precursors were ground again and cold-pressed under 30 MPa pressure into small thin pellets and annealed for 28 h at 1423 K followed by furnace cooling. All the samples are stable in the air at least up to several months. The crystal structure of $\text{Gd}_2\text{MgTiO}_6$ was identified by X-ray diffraction (XRD) at room temperature which is performed on a Rigaku-SmartLab-9KW diffractometer. XRD patterns have been collected in an angular range of 20–80° with a step of 0.02° on a grounded power sample. The microstructure, elements distribution and chemical compositions of $\text{Gd}_2\text{MgTiO}_6$ were analyzed on a JSM-7800F scanning electron microscope (SEM) with the Energy Dispersive X-Ray Spectroscopy (EDS) options using an accelerating voltage of 20 kV. The magnetic and MC properties of $\text{Gd}_2\text{MgTiO}_6$ were carried out using a superconducting quantum interference device (SQUID) magnetometer which was an option of magnetic properties measurement system (MPMS-7T, Quantum Design) in the tem-

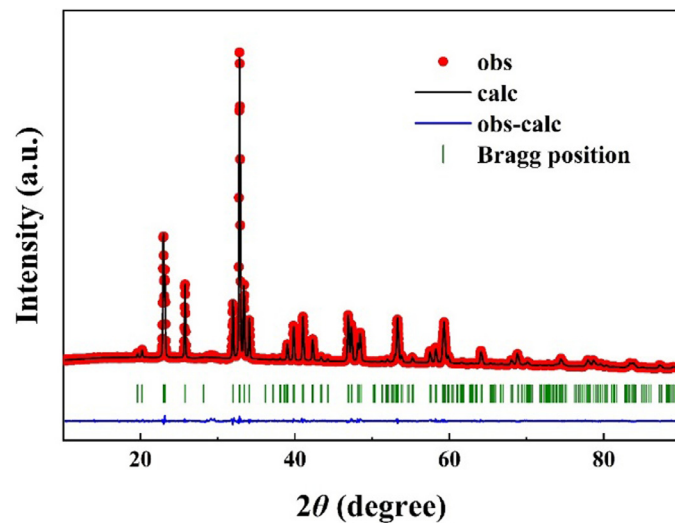


Fig. 1. The room temperature XRD pattern for $\text{Gd}_2\text{MgTiO}_6$ DP oxide.

perature range of 1.8–300 K and the magnetic field range of 0–7 T. The results of heat capacity under 0 and 7 T were measured by using the physical property measurement system (PPMS-9T, Quantum Design).

The atomic-level first-principles calculations based on density functional theory (DFT) were performed for unveiling the electronic and magnetic structure of $\text{Gd}_2\text{MgTiO}_6$ DP oxide. The standard Vienna *ab initio* Simulation Package (VASP) [43,44] was employed using plane waves to reproduce the one-electron wave functions with an energy of cutoff of 520 eV for constructing the basis set and projected augmented waves (PAW) pseudopotentials for all the species involved. And the valence electrons contributions in pseudopotentials are as [$5s^2$ $5p^6$ $4f^7$ $5d^1$ $6s^2$] for Gd, [$3s^2$] for Mg, [$3d^2$ $4s^2$] for Ti and [$2s^2$ $2p^4$] for O. Thus, the f electrons of Gd atom were firmly considered to accurately describe its magnetism. The electronic exchange and correlation were modeled by the Perdew-Burke-Ernzerhof (PBE) functional within the spin polarized generalized gradient approximation (GGA) [45]. Structural optimizations were performed using a conjugate gradient algorithm until the Hellman-Feynman forces were converged to less than 0.01 eV/Å and each self-consistent electronic loop converged to a tolerance smaller than 10^{-6} eV. And the k -points grid using Monkhorst-Pack method was set as $9 \times 9 \times 7$ for structural optimizations and static self-consistent calculations. To accurately compute the electronic properties, the k -points grid was set as $13 \times 13 \times 11$.

3. Results and discussion

The experimentally obtained XRD pattern for $\text{Gd}_2\text{MgTiO}_6$ powder sample along with the Rietveld refinement by the FULLPROF software [46] are plotted in Fig. 1. Both conventional perovskite-type $Pbnm$ and B -site ordered $P2_1/n$ (No. 14) space group were performed in the refinement. A better fitting result with the $P2_1/n$ space group is realized, and therefore the $\text{Gd}_2\text{MgTiO}_6$ crystallizes with monoclinic DP-type $P2_1/n$ symmetry. The refinement pattern shows phase-purity and crystallographic information of the oxide without any signature of impurity phases. The reasonable and goodness of fit of R_p , R_{wp} and R_F are evaluated to be 2.25, 1.67%, 2.18% and 1.45%, respectively. The lattice parameters of a , b , c and V are determined to be 5.3636(9) Å, 5.5997(2) Å, 7.6819(6) Å and 230.72(9) Å³, respectively. Moreover, the tolerance factor t , $t = \frac{r_{\text{RE}}+r_{\text{O}}}{\sqrt{2}(r_{\text{B}}+r_{\text{O}})}$ where r is ionic radius, can be used to evaluate the structural stability of perovskite-type oxides [47], which can only

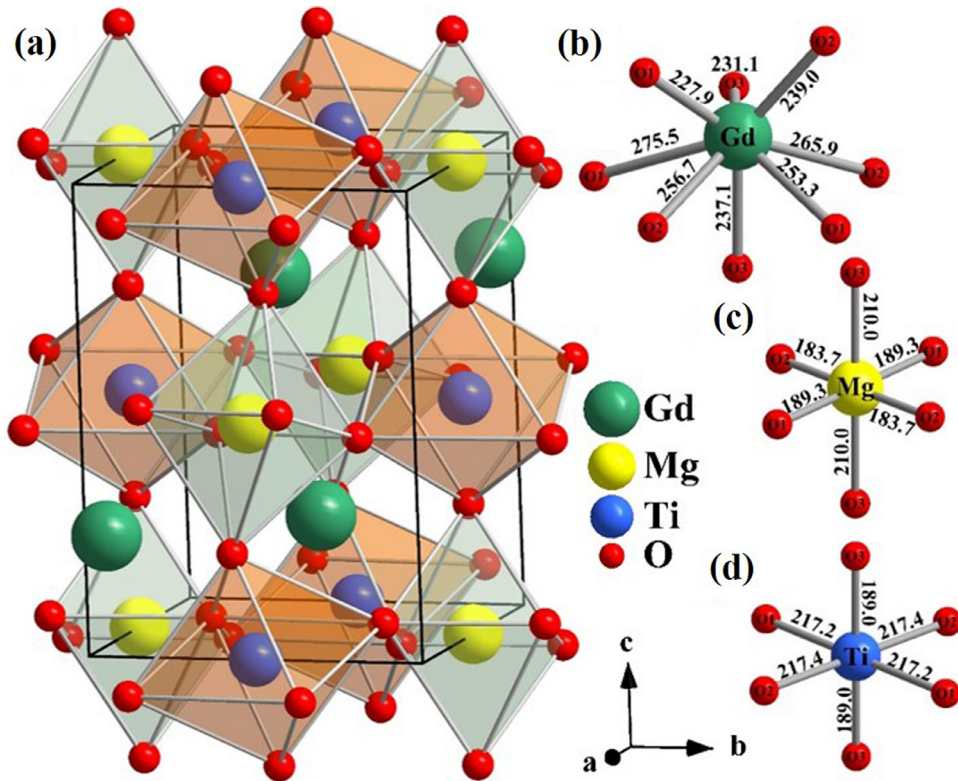


Fig. 2. The crystal structure (a) and atomic environment (b–d) for $\text{Gd}_2\text{MgTiO}_6$ DP oxide.

be stable with t ranging from 0.78 to 1.05. The value of t for $\text{Gd}_2\text{MgTiO}_6$ is 0.840, which also verifies the stability of DP-type crystal structure. Fig. 2(a–d) illustrate the detailed crystal structure of $\text{Gd}_2\text{MgTiO}_6$ DP oxide and near-neighbor environments of constituent elementals. In a single ordered unit, it has 20 independent atoms including two Mg atoms, two Ti atoms and twelve O atoms. Both Mg and Ti atoms coordinate with six O atoms forming the MgO_6 and TiO_6 octahedron, respectively. The bond distance ranges and average bond distance are 1.837–2.100 Å and 1.943 Å, as well as 1.890–2.174 Å and 2.079 Å for MgO_6 and TiO_6 , respectively. The O–Mg–O and O–Ti–O bond angles for MgO_6 and TiO_6 units range from 86.293° to 92.097° and 88.631° to 92.330°, respectively. Gd atom locates in the gap of $\text{MgO}_6/\text{TiO}_6$ octahedron forming the 8-coordination polyhedron with the bond distances from 2.279 Å to 2.755 Å. The occupation sites for Gd are 4e Wyckoff position, Mg and Ti ions are independent positions of 2d and 2c, while there exist three different O ions (O1, O2 and O3) and they are assumed three different 4e sites, respectively. Furthermore, the atomic environment information of the constituent elementals is summarized in Table 1 for $\text{Gd}_2\text{MgTiO}_6$ DP oxide. Fig. 3(a–e) illustrate the secondary electron SEM image of the typical microstructure together with the element EDS mapping results of $\text{Gd}_2\text{MgTiO}_6$ DP oxide. The prominent grain boundaries and high density nature confirm $\text{Gd}_2\text{MgTiO}_6$ DP oxide possessing pronounced polycrystalline nature. A number of EDS mapping analysis were performed and fractions confirmed the stoichiometric compositions of 19.36 mol%, 10.26 mol%, 11.42 mol% and 58.96 mol% for Gd, Ti, Mg and O atoms [as illustrated in Fig. 3(b–e)], respectively, which are rather close to the nominal atomic ratio 2:1:1:6 of synthesized $\text{Gd}_2\text{MgTiO}_6$ oxide.

Moreover, the *ab initio* calculations based on DFT can also provide valuable information of the crystal structure, charge transfer, distribution of magnetic moment and electronic structure by GGA method [43–45]. To further check the stability of the crystal structure, the ordered DP structure of monoclinic $P2_1/n$ space

Table 1
The structure parameters for $\text{Gd}_2\text{MgTiO}_6$ DP oxide.

Parameters	Wyckoff position	$\text{Gd}_2\text{MgTiO}_6$
Space group		$P2_1/n$ (No.14)
a (Å)		5.3636(9)
b (Å)		5.5997(2)
c (Å)		7.6819(6)
V (Å ³)		230.72(9)
Gd	4e (x, y, z)	
x		0.5152(4)
y		0.5605(5)
z		0.2462(6)
Mg	2d ($1/2, 0, 0$)	
Ti	2c ($0, 1/2, 0$)	
O ₁	4e (x, y, z)	
x		0.0988(8)
y		0.4713(3)
z		1/4
O ₂	4e (x, y, z)	
x		0.3207(7)
y		0.7281(4)
z		-0.0477(8)
O ₃	4e (x, y, z)	
x		0.4048(1)
y		0.9698(0)
z		0.2641(9)
c^2		3.05
R_p (%)		1.67
R_{wp} (%)		2.18
R_F (%)		1.45

group as detected by the XRD was selected as the initial structure for optimization. The lattice parameters a , b , c were determined as 5.34845 Å, 5.64097 Å and 7.71152 Å, respectively. The differences of optimized lattice parameters with the experimental results from XRD is less than 1%, which suggests the crystal structure by optimization is reasonable and available. Therefore, optimal structure was adopted in the following calculations. Fig. 4(a–c) il-

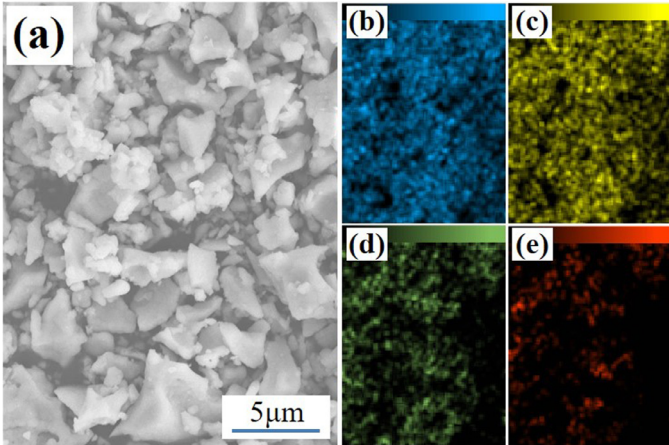


Fig. 3. The Scanning electron microscopy (SEM) image (a) and the distributions of Gd, Mg, Ti and O elements (b–e) for $\text{Gd}_2\text{MgTiO}_6$ DP oxide.

lustrate the difference charge density, which describe the charge transfer between metal ions and oxygen ions, where Fig. 4(c) illustrates the diagram at (100) cross section. Obviously, the charge is transferred from Ti^{4+} and Mg^{2+} to O^{2-} indicating the formation of ionic bond between Ti^{4+} (Mg^{2+}) and O^{2-} , whereas, the charge around Gd^{3+} is well localized, which indicates the Gd^{3+} probably has large local magnetic moment. Moreover, to determine the magnetic ground state of $\text{Gd}_2\text{MgTiO}_6$ DP oxide, the total energy (E_{tot}) at various potential magnetic structures were calculated. Due to the single magnetic component in this oxide, parallel magnetic state and three typical anti-parallel magnetic states were set for Gd^{3+} ions which are defined as FM, C-AFM, A-AFM and G-AFM states and the spin configuration which are given in Fig. 5(a–d), respectively. The values of E_{FM} , $E_{\text{C-AFM}}$, $E_{\text{A-AFM}}$ and $E_{\text{G-AFM}}$ are -99.37188 , -99.37631 , -99.37462 and -99.40434 eV/f.u., respectively. Apparently, the anti-parallel magnetic moment of Gd^{3+} ions have lower E_{tot} than parallel magnetic moment, which proves that the type of G-AFM coupling is present in $\text{Gd}_2\text{MgTiO}_6$ DP oxide. Moreover, the atomic magnetic moment of Gd^{3+} is determined as $7 \mu_B$. According to the state of anti-parallel magnetic ground state, the total density of states (DOS) of this oxide and partial DOS of each elements indicating the information of the electronic structure were

calculated by ab initio calculations with GGA+PBE method and the results are illustrated in Fig. 5(e). Obviously, a large band gap with the value of 2.977 eV proves the existence of semi-conductor characteristic in $\text{Gd}_2\text{MgTiO}_6$ DP oxide. And the 4f orbital of Gd^{3+} ions have obvious splitting behavior in the range of $\sim 3.003\text{--}3.854$ eV, which suggests each Gd^{3+} ion will spontaneously polarize to produce large magnetic moment. However, in the different positions of Gd^{3+} ions, the spins of electron are opposite, indicating that the magnetic moments generated spontaneously are canceled out, exhibiting the AFM ground state, which probably causes by hybridizing of electrons of Ti^{4+} and Gd^{3+} and proves the origin of AFM in $\text{Gd}_2\text{MgTiO}_6$ DP oxide. Moreover, the total DOS is mainly controlled by partial DOS of Gd^{3+} ions from ~ 3.003 to ~ 3.854 eV and by partial DOS of Ti^{4+} ions from ~ 5.403 to 7.226 eV, and hybridize with O^{2-} ions in the corresponding range. Below the fermi level, the total DOS is mainly contributed by O^{2-} ions, and Mg^{2+} and Ti^{4+} ions hybridize with O^{2-} ions in the range from ~ -4.195 to ~ 0 eV. Compared with Mg^{2+} and Ti^{4+} ions, partial DOS of Gd^{3+} and O^{2-} have a lower degree of overlap in the range of $-2.313\text{--}1.432$ eV.

To further probe the magnetic properties and MPT, the temperature dependent magnetic susceptibility $\chi (=M/H)$, the $\chi(T)$ curves, for $\text{Gd}_2\text{MgTiO}_6$ DP oxide was measured in terms of field cooling (FC) and zero-field cooling (ZFC) protocols with an external field H of 0.01 T, as illustrated in Fig. 6(a). The results suggest that c increases monotonously with the decrease of temperature, and exhibit a peak at around the Néel temperature $T_N \sim 3.3$ K, then decreases gradually with further increased of temperature, these behaviors suggesting a long-range MPT from paramagnetic to antiferromagnetic (PM to AFM) transition in $\text{Gd}_2\text{MgTiO}_6$ DP oxide. The FC and ZFC $\chi(T)$ curves are well overlapped in the whole measured temperature regime and thus there exists a negligible thermal hysteresis during their MPT in $\text{Gd}_2\text{MgTiO}_6$ DP oxide. The perfect reversibility of MPT is desirable for RE based materials, making the $\text{Gd}_2\text{MgTiO}_6$ DP oxide potentially interesting of practical cryogenic MR application. Furthermore, the $c(T)$ curves under various magnetic fields from 0.2, 1, 2, 3.5 and 5 T for $\text{Gd}_2\text{MgTiO}_6$ DP oxide are also illustrated in Fig. 6(a). Generally, the $c(T)$ curves show similar behaviors, except the peak temperature decreases slightly with increasing H , with H up to 3 T. Whereas, the c increases continuously with decreasing temperature under high magnetic fields of 3.5 and 5 T, and only some change in slope (as marked by arrows) at low temperature can be observed. These behaviors are

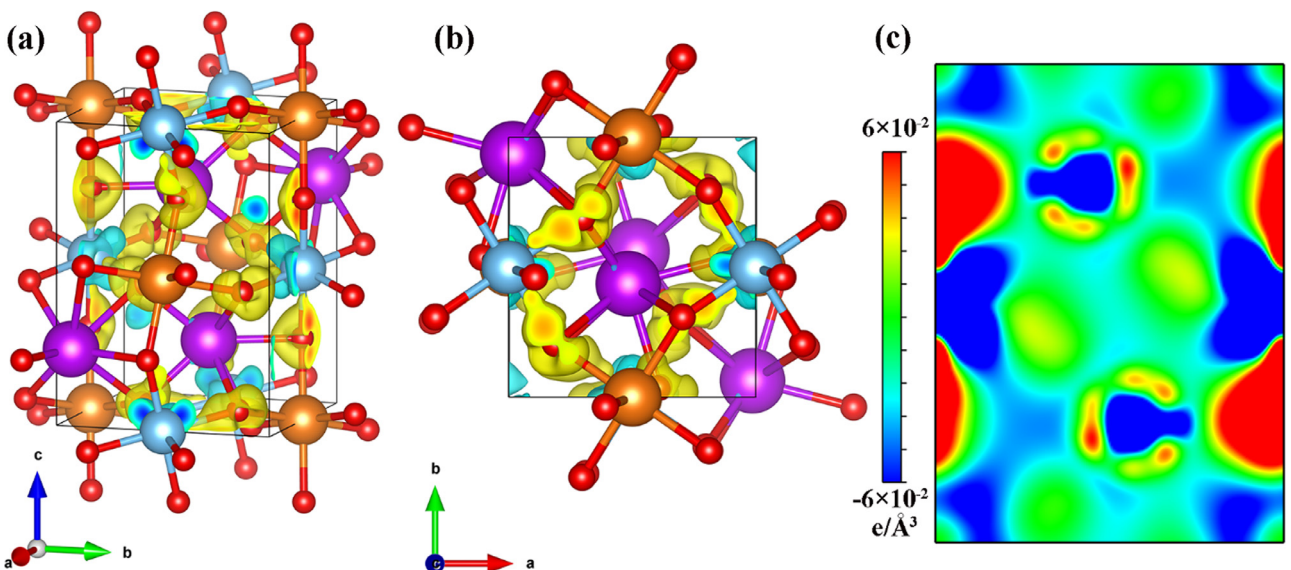


Fig. 4. The charge density difference with the 3D-display (a), along the c direction (b) and 2D-display in (100) plane (c) for $\text{Gd}_2\text{MgTiO}_6$ DP oxide.

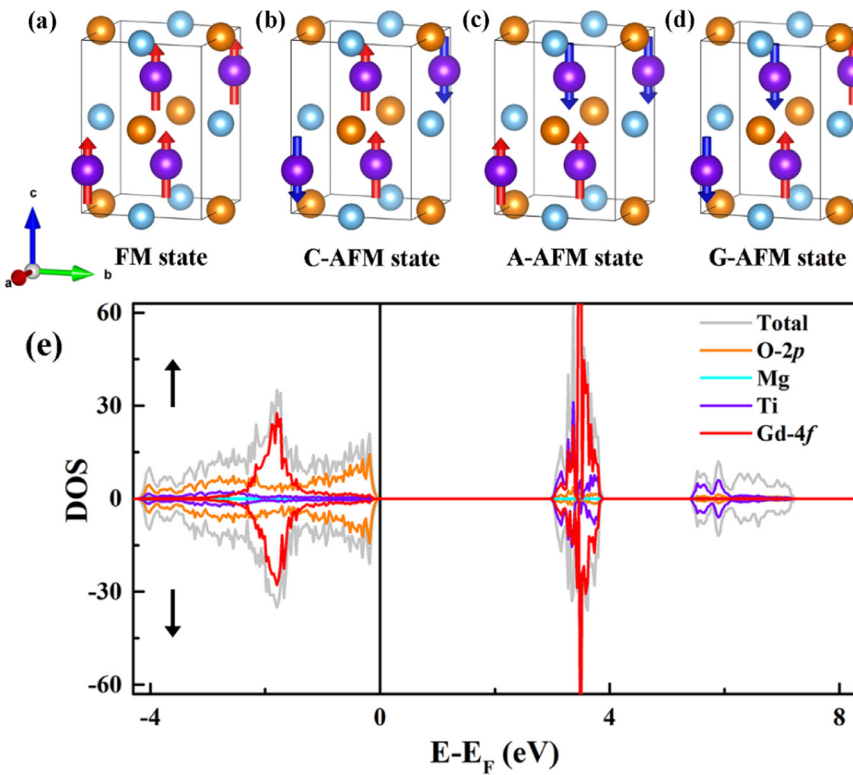


Fig. 5. (a-d): Four potential magnetic structure for Gd₂MgTiO₆ DP oxide. (e): The total DOS and partial DOS of O-2p, Mg, Ti, and Gd-f for Gd₂MgTiO₆ DP oxide.

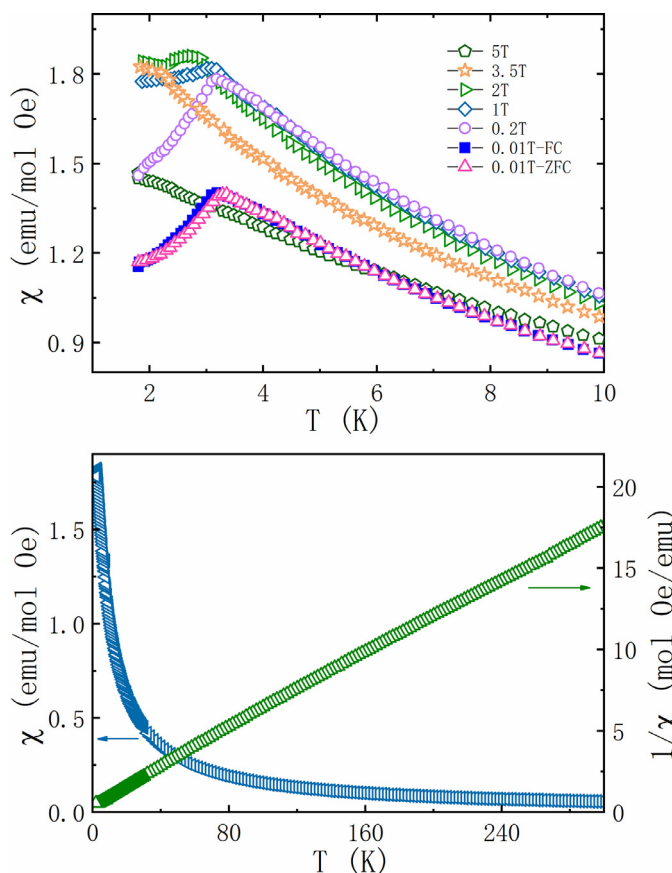


Fig. 6. (a): The $\chi(T)$ curves under various magentic fields including $c(T)$ curves with FC modes under 0.01 T for Gd₂MgTiO₆ DP oxide. (b): The $\chi(T)$ (left axis) and $1/\chi(T)$ (right axis) curves under $H = 1$ T for Gd₂MgTiO₆ DP oxide.

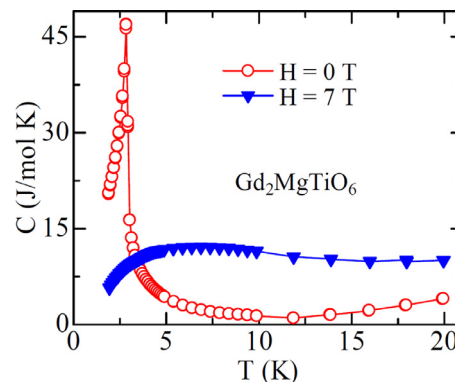


Fig. 7. The $C(T)$ curves under the magnetic fields of 0 and 7 T for Gd₂MgTiO₆ DP oxide.

fully consistent with the weakly interacting spins (dipolar). The $\chi(T)$ curve (left scale) and the reciprocal susceptibility $1/\chi(T)$ under $H = 1$ T are illustrated in Fig. 6(b). Clearly, the $1/\chi(T)$ curve nicely follows the Curie-Weiss law: $\chi(T) = C/(T - \theta_p)$, where θ_p denotes PM Curie temperature and C denotes Curie constant with $C = N(\mu_B \mu_{eff})^2 / 3\kappa_B$ (μ_{eff} : effective magnetic moment). Their linear fits yield negative θ_p value of -5.6 K which is indicating the AFM interaction at the ground state. The μ_{eff} value of 7.98 μ_B /f.u. which is very close to that of the theoretical calculated free Gd³⁺ ions (7.94 μ_B). These experimental observed magnetic properties for Gd₂MgTiO₆ DP oxide are consistent with those of theoretically predicated results. The temperature dependent heat capacity $C(T)$ curves for Gd₂MgTiO₆ DP oxide was measured under the magnetic fields of 0 and 7 T, as illustrated in Fig. 7. The observed pronounced peak around 3.0 K in the $C(T)$ curves under zero magnetic field is corresponding to the MPT which was confirmed by the magnetiza-

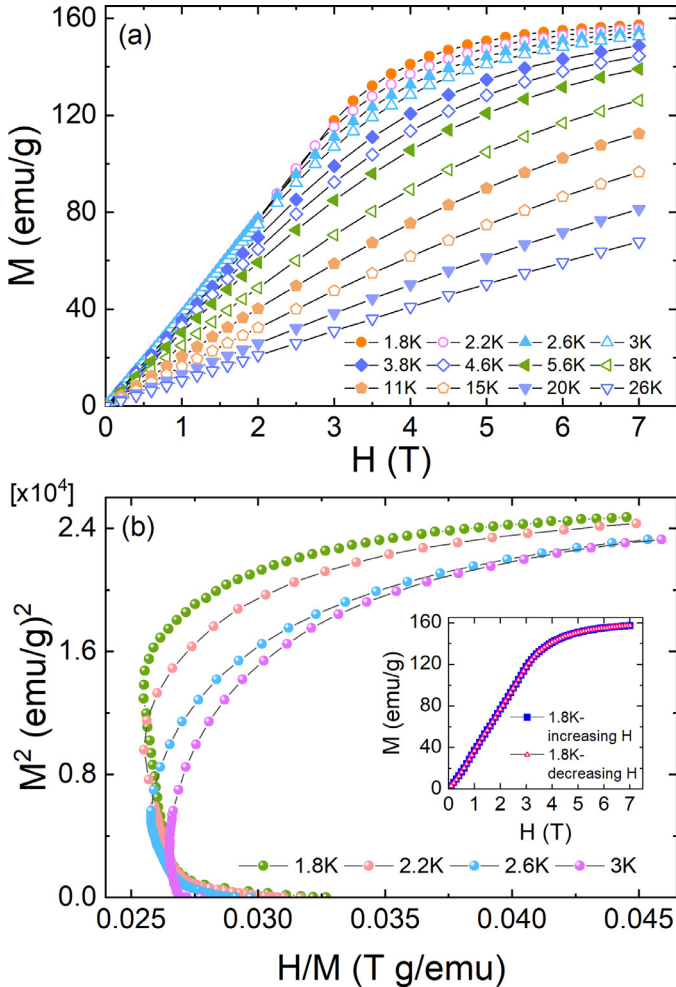


Fig. 8. The $M(H)$ curves (a) and the Arrott plots (M^2 - H/M) curves (b) for $\text{Gd}_2\text{MgTiO}_6$ DP oxide. Inset of (b) displays the $M(H)$ curves with increasing and decreasing magnetic field at 1.8 K.

tion measurement, whereas, only a broad hump can be observed in the $C(T)$ curves under the magnetic field of 7 T.

To further identify the MPT and MC properties of $\text{Gd}_2\text{MgTiO}_6$ DP oxide, series isothermal magnetization $M(H)$ curves were determined with applied H up to 7 T in the temperature range of 1.8–30 K, as illustrated in Fig. 8(a). The value of M at 1.8 K increases linearly with the increasing H up to 4 T, above which show a saturation behavior with the magnetic moment as high as $13.73 m_B$ per formula (two Gd^{3+} ions), which is almost 98% of the theoretical value of $7.0 \mu_B$ for a non-interacting Gd^{3+} single ion. Since the Ti^{4+} and Mg^{2+} sub-lattices have no contribution on the overall magnetism, thus the Gd^{3+} sub-lattice should be in charge of the magnetism of $\text{Gd}_2\text{MgTiO}_6$ DP oxide. In addition, $M(H)$ curves at 1.8 K with increasing H and decreasing are illustrated in the inset of Fig. 8(b). Both curves overlap well with each other during the whole measured magnetic field range, suggesting no magnetic hysteresis in $\text{Gd}_2\text{MgTiO}_6$ DP oxide. Accordingly, a giant reversible MC effect would be happened at low temperature in $\text{Gd}_2\text{MgTiO}_6$ which is of great importance for practical MR application. It is well accepted that MC effect of the magnetic solids has strong relationship with the MPT, it is therefore crucial to confirm the orders of the corresponding MPT for $\text{Gd}_2\text{MgTiO}_6$ DP oxide. The MPT nature is further confirmed by using the Arrott plots based on the Banerjee criterion [48] which were constructed from the already recorded sets of $M(H)$ curves. In principle, the negative or positive

slopes in M^2 vs. H/M plots are indicative of a first or second-order phase transition (F/SOPT) for a magnetic solid. The curves at low temperatures of 1.8, 2.2, 2.6 and 3 K show negative slopes [as illustrated in Fig. 8(b)], which probably indicates the occurrence of FOPT in $\text{Gd}_2\text{MgTiO}_6$ DP oxide.

Generally, the investigation on the MC effect is based on the analysis of the temperature and magnetic field change (ΔH) dependences of magnetic entropy change ($-\Delta S_M$), which is derived according to the Maxwell thermodynamic relation by Eqs. (1) and (2) [13–16]:

$$\Delta S_M(T, H) = S(M, H) - S(M, 0) = \int_0^H \left(\frac{\partial M(T, H)}{\partial T} \right) H dH \quad (1)$$

and from the temperature dependence of the heat capacity (as illustrated in Fig. 7) under the zero magnetic field $C(T, H_0)$ and applied magnetic field $C(T, H_1)$ by using the equation,

$$\Delta S_M(T, \Delta H) = [S(T)_{H_1} - S(T)_{H_0}]_T = \int_0^T \frac{C(T, H_1) - C(T, H_0)}{T} dT, \quad (2)$$

respectively. The evaluated temperature dependence of $-\Delta S_M$ calculated from $M(H, T)$ and $C(T, H)$ data for $\text{Gd}_2\text{MgTiO}_6$ DP oxide are all illustrated in Fig. 9(a) under several typical ΔH up to 0–7 T. The results obtained by using both methods are generally in consistent with each other. The $-\Delta S_M$ values for $\text{Gd}_2\text{MgTiO}_6$ DP oxide rise progressively with decreasing temperature above T_N and increase gradually with increasing H , which is in accordance with the usual behavior of MC effects. It is well known that the commercial permanent magnet is difficult to generate the magnetic field higher than 2 T, large values of $-\Delta S_M$ under low magnetic field changes are feasible to design the MR cycle using permanent magnets. The maximum value of positive $-\Delta S_M$ ($-\Delta S_M^{\max}$) is 6.06 J/kgK with ΔH of 0–2 T. The moderate values of $-\Delta S_M$ under low ΔH would limit its practical application by using the permanent magnet. Moreover, we should note that the value $-\Delta S_M^{\max}$ increases continuously with increasing ΔH , as illustrated in Fig. 9(b). The values of $-\Delta S_M^{\max}$ under ΔH of 0–7 T are as high as 46.21 and 43.46 J/kgK calculated from $M(H, T)$ and $C(T, H)$ data, respectively. In the below, we use the ΔS_M data obtained from the $M(H, T)$ for comparison with other MC materials which were calculated in the similar way. This value is much larger than that of the commercialized famous gadolinium gallium garnet $\text{Gd}_3\text{Ga}_5\text{O}_{12}$ (abbreviated as GGG) developed has long been deemed as the benchmark cryogenic MC material with $-\Delta S_M^{\max}$ of 38.4 J/kgK under ΔH of 0–7 T around 2.0 K [13,49]. Moreover, this value at 0–7 T is still far below the theoretical limitation $-\Delta S_{M\text{-limit}}$ which is usually produced by using the contribution of the uncoupled Gd^{3+} ions and can be approximately evaluated by the Eq. (3) [17]:

$$-\Delta S_{M\text{-limit}} = R \ln(2S + 1) \quad (3)$$

in which R presents the gas constant, and S presents the half-filled 4f orbital of Gd^{3+} ions with a large spin state of $S = 7/2$. The calculated upper limit of $-\Delta S_{M\text{-limit}}$ is 71.59 J/kgK for $\text{Gd}_2\text{MgTiO}_6$ DP oxide. Such differences would be probably related to the additional internal entropy loss from the phonon contribution and the limitation of ΔH for present measurements. By considering the fact of that the $-\Delta S_M^{\max}$ value does not show any saturation trends with ΔH up to 0–7 T, thus a much larger $-\Delta S_M^{\max}$ would be attained for $\text{Gd}_2\text{MgTiO}_6$ DP oxide by further increasing ΔH . Moreover, the temperature-averaged magnetic entropy change, TEC , has been recently introduced as an important figure of merit [50] to further examine the performances of the MC materials. The TEC considers the mean value at the certain temperature span (ΔT_{lift}) under a

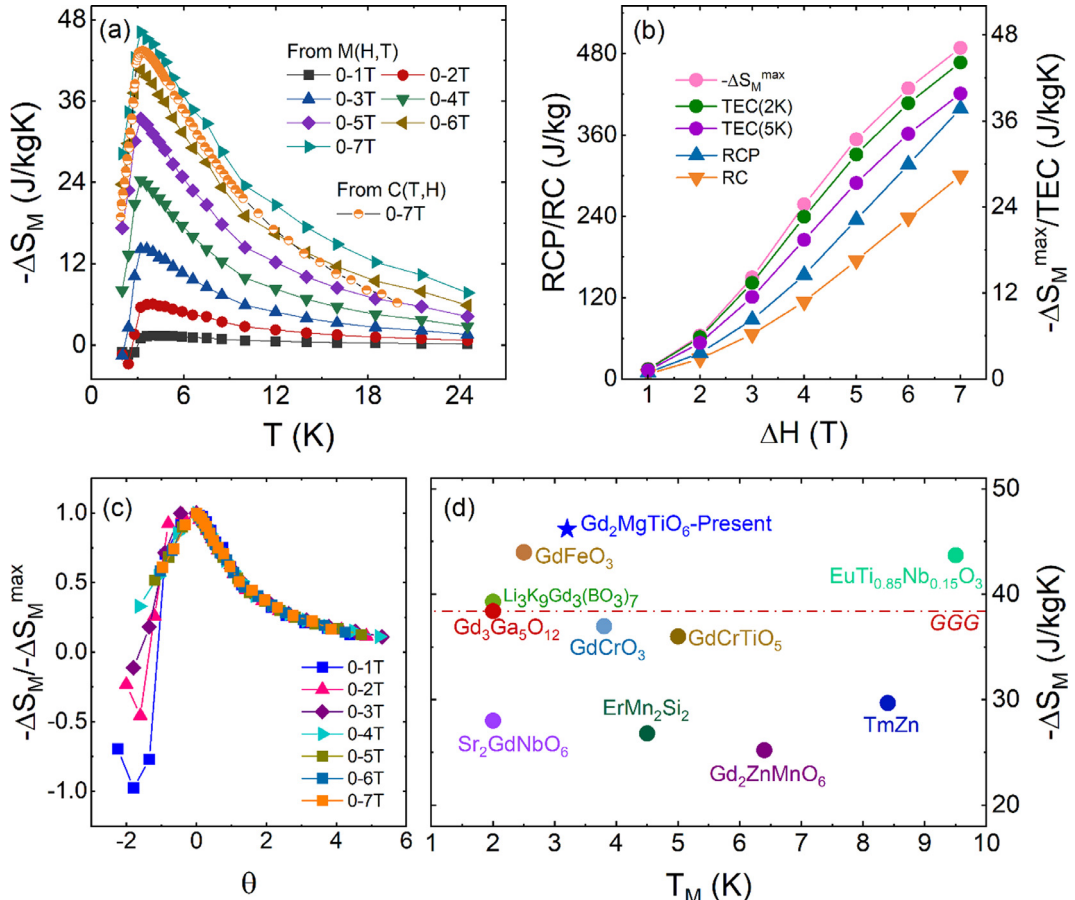


Fig. 9. (a): The $-\Delta S_M(T)$ curves from 0 to 1 to 0–7 T of $\text{Gd}_2\text{MgTiO}_6$ DP oxide. (b): The magnetic field change ΔH dependence of $\text{TEC}(2/5 \text{ K})$ and $-\Delta S_M^{\max}$ together with the RCP and RC for $\text{Gd}_2\text{MgTiO}_6$ DP oxide. (c): The $(\Delta S_M(T)/\Delta S_M^{\max})$ vs. rescaled temperature (θ) curves of $\text{Gd}_2\text{MgTiO}_6$ DP oxide. (d): The comparison of $-\Delta S_M^{\max}$ for the present $\text{Gd}_2\text{MgTiO}_6$ DP oxide and some famous RE-based MC materials with working temperature below 10 K.

fixed ΔH and has been described by Eq. (4)

$$\text{TEC}(\Delta T_{\text{lift}}) = \frac{1}{\Delta T_{\text{lift}}} \max_{T_{\text{mid}}} \left\{ \int_{T_{\text{mid}} - \frac{\Delta T_{\text{lift}}}{2}}^{T_{\text{mid}} + \frac{\Delta T_{\text{lift}}}{2}} \Delta S_M(T) \Delta H, T dT \right\} \quad (4)$$

T_{mid} is the value of the temperature at the center of the average and selected the largest value for a given ΔT_{lift} . Two different ΔT_{lift} values of 2 K and 5 K are chosen to evaluate the value of TEC for the $\text{Gd}_2\text{MgTiO}_6$ DP oxide. The resulting values of $\text{TEC}(2 \text{ K})$ and (5 K) values at ΔH of 0–7 T are 44.15 and 39.84 J/kgK for $\text{Gd}_2\text{MgTiO}_6$, respectively. Similar ΔH dependent trend of $\text{TEC}(2 \text{ K})$, $\text{TEC}(5 \text{ K})$ and $-\Delta S_M^{\max}$ for $\text{Gd}_2\text{MgTiO}_6$ DP oxide can be observed, as given in Fig. 9(b). Obviously, the values of $\text{TEC}(2 \text{ K})$ are much closer to the calculated $-\Delta S_M^{\max}$ as compared to the values calculated for $\text{TEC}(5 \text{ K})$. The reason should ascribe to the fact that the peak width is slightly narrow, thus a small ΔT_{lift} will result in little reduction of the TEC . Moreover, the relative cooling power (RCP) as expressed by Eq. (5) and refrigerant capacity (RC) as expressed by Eq. (6) are another two well-known correlated factors [24–26] which enable us to evaluate the amounts of energy that can be transferred between the cold end and hot end in an ideal MR cycle.

$$\text{RCP} = |\Delta S_M^{\max}| \times \delta T_{\text{FWHM}} \quad (5)$$

$$\text{RC} = \int_{T_{\text{cold}}}^{T_{\text{hot}}} |\Delta S_M(T)| dT, \quad (6)$$

where integration limits (T_{cold} and T_{hot}) represent the two sides at $\frac{1}{2}|\Delta S_M^{\max}|$ value of $-\Delta S_M(T)$ profile, and $\delta T_{\text{FWHM}} (= T_{\text{hot}} - T_{\text{cold}})$.

The RC and RCP against ΔH are also displayed in the right-hand side axis of Fig. 9(b). Significantly, RC and RCP show similar increasing tendency of continuous increase with ΔH . The calculated RCP/RC values are 38.77/30.04 and 399.05/300.03 J/kg for $\text{Gd}_2\text{MgTiO}_6$ DP oxide, with ΔH of 0–2 and 0–7 T, respectively. For a more direct observation of MC performances, we use the $-\Delta S_M^{\max}$ values for judgement. A comparison of representative of recently reported famous RE-based MC materials [38,39,49,51–57] with the working temperatures below 10 K of their $-\Delta S_M$ under ΔH of 0–7 T have been summarized in Fig. 9(d). As can be seen, the $-\Delta S_M^{\max}$ is dramatically as high as 46.21 J/kgK for $\text{Gd}_2\text{MgTiO}_6$ DP oxide, approximately 20% higher than that of the commercialized magnetic refrigerant GGG (38.4 J/kgK under ΔH of 0–7 T) [49], and outperform most of the famous recently reported MC materials at cryogenic temperature region. The present results indicate that $\text{Gd}_2\text{MgTiO}_6$ DP oxide is an excellent MC material working at the temperature region for the liquefaction of helium.

Additionally, a phenomenological constructed universal curve [58,59] has been proposed and widely applied by normalizing the $-\Delta S_M(T)$ curve to its peak $-\Delta S_M^{\max}$ as $\Delta S' (= \Delta S_M(T)/\Delta S_M^{\max})$, and rescaling the temperature axis to $(T - T_{\text{peak}})/(T_{\text{r1}} - T_{\text{peak}})$ as θ , in which T_{peak} denotes the temperature of $-\Delta S_M^{\max}$, and T_{r1} and T_{r2} denote the temperatures corresponding to $0.6 \times \Delta S_M^{\max}$ above and below T_{peak} for each ΔH , respectively, and is expressed by Eq. (7):

$$\theta = \begin{cases} -(T - T_{\text{peak}})/(T_{\text{r1}} - T_{\text{peak}}), & T \leq T_{\text{peak}} \\ (T - T_{\text{peak}})/(T_{\text{r2}} - T_{\text{peak}}), & T > T_{\text{peak}}, \end{cases} \quad (7)$$

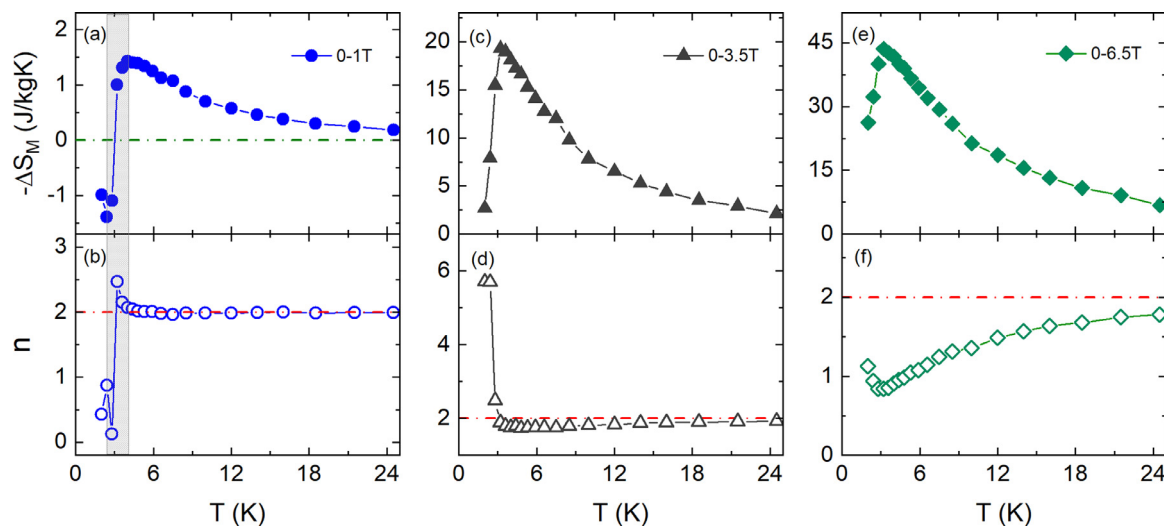


Fig. 10. The temperature dependence of ΔS_M and corresponding exponent n under different fields of 0–1, 0–3.5 and 0–6.5 T for $\text{Gd}_2\text{MgTiO}_6$ DP oxide.

The processed $\Delta S'(\theta)$ curves for $\text{Gd}_2\text{MgTiO}_6$ DP oxide are depicted in Fig. 9(c). It can be notice that all the $\Delta S'(\theta)$ curves show clear branches below MPT, whereas a single master curve behavior can be observed above MPT, which resemble the existing both first-order and second-order MPTs for present $\text{Gd}_2\text{MgTiO}_6$ DP oxide at different temperature zones, respectively.

Furthermore, the order of MPT can be checked by novel MC criterion, the field dependence exponent of ΔS_M which was computed according to the Eq. (8) [60–62]:

$$n(T, H) = \frac{d \ln |\Delta S_M|}{d \ln H} \quad (8)$$

Fig. 10 illustrates the temperature dependence of ΔS_M and exponent n under three different ΔH of 0–1, 0–3.5 and 0–6.5 T for $\text{Gd}_2\text{MgTiO}_6$ DP oxide. Previous investigation suggested that, a clear overshoot of n above 2 should be existed in the $n(T)$ curves for a FOPT material around its transition temperature [60–62]. For ΔH of 0–1.5 T, an obvious characteristic spike can be observed as displayed in the shaded gray zone, suggesting the switching from inverse to conventional MCE. The n value just shows a small increase but below 2 within the inverse MCE region, which is ascribed to the ultralow MPT of $\text{Gd}_2\text{MgTiO}_6$ oxide, as shown in Fig. 10(a) and (b). For ΔH of 0–3.5 T, the overshoot feature (n above 2) can be clearly noted at low temperatures, which indicates the FOPT nature of the MPT, as shown in Fig. 10(c) and (d). In parallel, there is not any overshoot of $n > 2$ near the MPT for ΔH of 0–6.5 T, indicating that the nature of SOPT, as shown in Fig. 10(e) and (f). These results are consistent well with those obtained by Banerjee criterion.

4. Conclusions

In summary, high quality single phased polycrystalline $\text{Gd}_2\text{MgTiO}_6$ oxide with a B -site ordered monoclinic $P2_1/n$ (No. 14) DP type crystal structure has been successfully fabricated. A combined theoretical and experimental investigation have been carried out in detail in terms of the crystal structure, magnetism, MPT and MC performances. The $\text{Gd}_2\text{MgTiO}_6$ oxide is belonging to a B -site ordered monoclinic double perovskite (DP) type structure and has AFM interaction and semi-conductor characteristic at ground state. Moreover, a giant reversible cryogenic MC effect together with outstanding MC performances at around T_N of 3.3 K have been found in $\text{Gd}_2\text{MgTiO}_6$ DP oxide with the $-\Delta S_M^{\max}$, $TEC(2 \text{ K})$, RCP and RC values as high as 46.21 and 44.15 J/kgK ,

399.04 and 300.27 J/kg with ΔH of 0–7 T, respectively. Evidently, these MC parameters of $\text{Gd}_2\text{MgTiO}_6$ is better than those of recently reported famous cryogenic MC materials and also the commercial gadolinium gallium garnet (GGG), making the $\text{Gd}_2\text{MgTiO}_6$ DP oxide attractive for practical cryogenic MR application.

Declaration of Competing Interest

The authors declare that they have no known competing financial interests or personal relationships that could have appeared to influence the work reported in this paper.

Acknowledgments

The present work was financially supported by the National Natural Science Foundation of China (Grant No. 52071197), the “Pioneer” and “Leading Goose” R&D Program of Zhejiang (No. 2022C01230), the Science and Technology Committee of Shanghai Municipality (Nos. 19ZR1418300 and 19DZ2270200), and Independent Research and Development Project of State Key Laboratory of Advanced Special Steel, Shanghai Key Laboratory of Advanced Ferrometallurgy, Shanghai University (SKLASS 2021-Z05).

References

- [1] O. Guttfleisch, M.A. Willard, E. Brück, C.H. Chen, S.G. Sankar, J.P. Liu, Magnetic materials and devices for the 21st century: stronger, lighter, and more energy efficient, *Adv. Mater.* 23 (2011) 821–842.
- [2] X. Moya, S. Kar-Narayan, N.D. Mathur, Caloric materials near ferroic phase transitions, *Nat. Mater.* 13 (2014) 439–450.
- [3] I. Takeuchi, K. Sandemana, Solid-state cooling with caloric materials, *Phys. Today* 68 (2015) 48–54.
- [4] T. Gottschall, A. Gracia-Condal, M. Fries, A. Taubel, L. Pfeuffer, L. Mañosa, A.I. Planes, K.P. Skokov, O. Guttfleisch, A multicaloric cooling cycle that exploits thermal hysteresis, *Nat. Mater.* 17 (2018) 929.
- [5] D.Y. Cong, W. Xiong, A. Planes, Y. Ren, L. Mañosa, P. Cao, Z. Nie, X. Sun, Z. Yang, X. Hong, Y.D. Wang, Colossal elastocaloric effect in ferroelastic Ni-Mn-Ti alloys, *Phys. Rev. Lett.* 122 (2019) 255703.
- [6] B. Li, Y. Kawakita, S. Ohira-Kawamura, T. Sugahara, H. Wang, J. Wang, Y. Chen, S.I. Kawaguchi, S. Kawaguchi, K. Ohara, K. Li, D. Yu, R. Mole, T. Hattori, T. Kikuchi, S. Yano, Z. Zhang, Z. Zhang, W. Ren, S. Lin, O. Sakata, K. Nakajima, Z.D. Zhang, Colossal barocaloric effects in plastic crystals, *Nature* 567 (2019) 506–510.
- [7] Y. Wang, L. Wang, J. Xia, Z. Lai, G. Tian, X. Zhang, Z. Hou, X. Gao, W. Mi, M. Zeng, G. Zhou, G. Yu, G. Wu, Y. Zhou, W. Wang, X.X. Zhang, J.M. Liu, Electric-field-driven non-volatile multi-state switching of individual skyrmions in a multiferroic heterostructure, *Nat. Commun.* 11 (2020) 3577.
- [8] L. Hu, L. Cao, L. Li, J. Duan, X. Liao, F. Long, J. Zhou, Y. Xiao, Y. Zeng, S. Zhou, Two-dimensional magneto-photoconductivity in non-van der Waals manganese selenide, *Mater. Horiz.* 8 (2021) 1286–1296.

- [9] Z. Hou, L. Li, C. Liu, X. Gao, Z. Ma, Y. Peng, M. Yan, X. Zhang, J. Liu, Emergence of room temperature stable skyrmionic bubbles in the rare earth based REMn_2Ge_2 ($\text{RE} = \text{Ce}, \text{Pr}$, and Nd) magnets, *Mater. Today Phys.* 17 (2021) 100341.
- [10] L. Hu, J. Zhou, Z. Hou, W. Su, B. Yang, L. Li, M. Yan, Polymer-buried van der Waals magnets for promising wearable room-temperature spintronics, *Mater. Horiz.* 8 (2021) 3306–3314.
- [11] V. Provenszno, A. Shapiro, R. Shul, Reduction of hysteresis losses in the magnetic refrigerant $\text{Gd}_5\text{Ge}_2\text{Si}_2$ by the addition of iron, *Nature* 429 (2004) 853–857.
- [12] K.A. Gschneidner, V.K. Pecharsky, A.O. Tsokol, Recent developments in magnetocaloric materials, *Rep. Prog. Phys.* 68 (2005) 1479–1539.
- [13] E. Liu, W. Wang, L. Feng, G. Li, J. Chen, H. Zhan, G. Wu, C. Jiang, H. Xu, F. Boer, Stable magnetostructural coupling with tunable magnetoresponsive effects in hexagonal phase-transition ferromagnets, *Nat. Commun.* 3 (2012) 873.
- [14] J. Liu, T. Gottschal, K. Skokov, J. Moore, O. Gutfleisch, Giant magnetocaloric effect driven by structural transitions, *Nat. Mater.* 11 (2012) 620–626.
- [15] V. Franco, J. Blázquez, J. Iplus, J. Law, L. Ramírez, A. Comde, Magnetocaloric effect: from materials research to refrigeration devices, *Progr. Mater. Sci.* 93 (2018) 112–232.
- [16] X. Zheng, X. Kong, Z. Zheng, L. Long, L. Zheng, High-nuclearity lanthanide-containing clusters as potential molecular magnetic coolers, *Acc. Chem. Res.* 51 (2018) 517–525.
- [17] L.M. Ramírez, C.R. Muñiz, J.Y. Law, V. Franco, K. Skokov, O. Gutfleisch, Tunable first order transition in $\text{La}(\text{Fe,Cr,Si})_{13}$ compounds: retaining magnetocaloric response despite a magnetic moment reduction, *Acta Mater.* 175 (2019) 406–414.
- [18] Y. Ouyang, M.X. Zhang, A. Yan, W. Wang, F. Guillou, J. Liu, Plastically deformed La–Fe–Si: microstructural evolution, magnetocaloric effect and anisotropic thermal conductivity, *Acta Mater.* 187 (2020) 1–11.
- [19] Z. Ma, X. Dong, Z.Z. Zhang, L.W. Li, Achievement of promising cryogenic magnetocaloric performances in $\text{La}_{1-x}\text{Pr}_x\text{Fe}_{12}\text{B}_6$ compounds, *J. Mater. Sci. Technol.* 92 (2021) 138–142.
- [20] N. Terada, H. Mamiya, High-efficiency magnetic refrigeration using holmium, *Nat. Commun.* 12 (2021) 1212.
- [21] Y. Li, L. Qin, S. Huang, L. Li, Enhanced magnetocaloric performances and tunable martensitic transformation in $\text{Ni}_{35}\text{Co}_{15}\text{Mn}_{35-x}\text{Fe}_x\text{Ti}_{15}$ all-d-metal Heusler alloys by chemical and physical pressures, *Sci. China Mater.* (2022), doi:10.1007/s40843-021-1747-3.
- [22] J.Y. Law, A.D. García, L.M.M. Ramírez, V. Franco, Increased magnetocaloric response of FeMnNiGeSi high-entropy alloys, *Acta Mater.* 212 (2021) 116931.
- [23] Y. Yuan, Y. Wu, X. Tong, H. Wan, Z. Liu, H. Suog, Z. Liu, Rare-earth high-entropy alloys with giant magnetocaloric effect, *Acta Mater.* 125 (2017) 481–489.
- [24] Y.K. Zhang, Review of the structural, magnetic and magnetocaloric properties in ternary rare earth $\text{RE}_2\text{T}_2\text{X}$ type intermetallic compounds, *J. Alloy. Compd.* 787 (2019) 1173–1186.
- [25] L.W. Li, M. Yan, Recent progresses in exploring the rare earth based intermetallic compounds for cryogenic magnetic refrigeration, *J. Alloy. Compd.* 823 (2020) 153810.
- [26] Y. Zhang, H. Li, J. Wang, Z. Ren, G. Wilde, Structure and cryogenic magnetic properties in $\text{Ho}_2\text{BaCuO}_5$ cuprate, *Ceram. Int.* 44 (2018) 1991–1994.
- [27] F. Guillou, A.K. Pathak, D. Paudyal, Y. Mudryk, F. Wilhelm, A. Rogalev, V.K. Pecharsky, Non-hysteretic first-order phase transition with large latent heat and giant low-field magnetocaloric effect, *Nat. Commun.* 9 (2018) 2925.
- [28] L. Li, C. Xu, Y. Yuan, S. Zhou, Achievement of a table-like magnetocaloric effect in the dual-phase $\text{ErZn}_2/\text{ErZn}$ composite, *Mater. Res. Lett.* 6 (2018) 67–71.
- [29] Y. Zhang, B. Wu, D. Guo, J. Wang, Z. Ren, Magnetic properties and promising cryogenic magneto-caloric performances of $\text{Gd}_{20}\text{Ho}_{20}\text{Tm}_{20}\text{Cu}_{20}\text{Ni}_{20}$ amorphous ribbons, *Chin. Phys. B* 30 (2021) 017501.
- [30] J. Ćwik, Y. Koshkid'ko, N. Kolchugina, K. Nenkov, N.A. de Oliveira, Thermal and magnetic effects in quasi-binary $\text{Tb}_{1-x}\text{Dy}_x\text{Ni}_2$ ($x = 0.25, 0.5, 0.75$) intermetallics, *Acta Mater.* 173 (2019) 27–33.
- [31] Y. Zhang, J. Zhu, S. Li, J. Wang, Z. Ren, Achievement of giant cryogenic refrigerant capacity in quinary rare-earths based high-entropy amorphous alloy, *J. Mater. Sci. Technol.* 102 (2022) 66–71.
- [32] Y. Zhang, J. Zhu, S. Li, Z. Zhang, J. Wang, Z. Ren, Magnetic properties and promising cryogenic magnetocaloric performances in the antiferromagnetic GdFe_2Si_2 compound, *Sci. China Mater.* 65 (2021) In press, doi:10.1007/s40843-021-1967-5.
- [33] X. Chen, J. Xu, Y.S. Xu, F. Luo, Y.P. Du, Rare earth double perovskites: a fertile soil in the field of perovskite oxides, *Inorg. Chem. Front.* 6 (2019) 2226–2238.
- [34] W.J. Yin, B. Weng, J. Ge, Q. Sun, Z. Li, Y. Yan, Oxide perovskites, double perovskites and derivatives for electrocatalysis, photocatalysis, and photovoltaics, *Energy Environ. Sci.* 12 (2019) 442–462.
- [35] T. Tiittanen, S. Vasala, M. Karppinen, Assessment of magnetic properties of $\text{A}_2\text{B}'\text{O}_6$ double perovskites by multivariate data analysis techniques, *Chem. Commun.* 55 (2019) 1722–1725.
- [36] Y.K. Zhang, B. Zhang, S. Li, J. Zhu, B. Wu, J. Wang, Z. Ren, Cryogenic magnetic properties and magnetocaloric effects (MCE) in B-site disordered $\text{RE}_2\text{CuMnO}_6$ ($\text{RE} = \text{Gd}, \text{Dy}, \text{Ho}$ and Er) double perovskites (DP) compounds, *Ceram. Int.* 47 (2021) 18205–18212.
- [37] B. Wu, Y. Zhang, D. Guo, J. Wang, Z. Ren, Structure, magnetic properties and cryogenic magneto-caloric effect (MCE) in $\text{RE}_2\text{FeAlO}_6$ ($\text{RE} = \text{Gd}, \text{Dy}, \text{Ho}$) oxides, *Ceram. Int.* 47 (2021) 6290–6297.
- [38] L.W. Li, P. Xu, S.K. Ye, Y. Li, D. Liu, D.X. Huo, M. Yan, Magnetic properties and excellent cryogenic magnetocaloric performances in B-site ordered $\text{RE}_2\text{ZnMnO}_6$ ($\text{RE} = \text{Gd}, \text{Dy}$ and Ho) perovskites, *Acta Mater.* 194 (2020) 354–365.
- [39] P. Xu, Z.P. Ma, P. Wang, H. Wang, L. Li, Excellent cryogenic magnetocaloric performances in ferromagnetic $\text{Sr}_2\text{GdBnO}_6$ double perovskite compound, *Mater. Today Phys.* 20 (2021) 100470.
- [40] P. Gao, Z. Zhou, P. Dong, Q. Li, H. Li, J. Wang, Z. Zhou, M. Xia, Tuning the luminescence properties of blue and far-red dual emitting $\text{Gd}_2\text{MgTiO}_6:\text{Bi}^{3+}, \text{Cr}^{3+}$ phosphor for LED plant lamp, *J. Am. Ceram. Soc.* 104 (2021) 6444–6454.
- [41] D. Stefańska, B. Bondzior, T.H.Q. Vu, M. Grodzicki, P.J. Dereń, Temperature sensitivity modulation through changing the vanadium concentration in a $\text{La}_2\text{MgTiO}_6:\text{V}^{5+}, \text{Cr}^{3+}$ double perovskite optical thermometer, *Dalton Trans.* 50 (2021) 9851–9857.
- [42] S. Gai, H. Zhu, P. Gao, C. Zhou, Z. Kong, M.S. Molokeev, Z. Qi, Z. Zhou, M. Xia, Structure analysis, tuning photoluminescence and enhancing thermal stability on Mn^{4+} -doped $\text{La}_{2-x}\text{Y}_x\text{MgTiO}_6$ red phosphor for agricultural lighting, *Ceram. Int.* 46 (2020) 20173–20182.
- [43] G. Kresse, J. Furthmüller, Efficient iterative schemes for ab initio total-energy calculations using a plane-wave basis set, *Phys. Rev. B* 54 (1996) 11169–11186.
- [44] R.A. Evarestov, V.P. Smirnov, Modification of the Monkhorst-Pack special points meshes in the Brillouin zone for density functional theory and Hartree-Fock calculations, *Phys. Rev. B* 70 (2004) 233101.
- [45] J.P. Perdew, K. Burke, M. Ernzerhof, Generalized gradient approximation made simple, *Phys. Rev. Lett.* 77 (1996) 3865–3868.
- [46] J. Rodriguez-Carvajal, FULLPROF: A Rietveld and Pattern Matching Analysis Program, Laboratoire Leon Brillouin CEA-CNRS, France, 2007.
- [47] C. Bartel, C. Suton, B. Goldsmith, R. Oyang, C. Musgrave, M. Scheffler, New tolerance factor to predict the stability of perovskite oxides and halides, *Sci. Adv.* 5 (2019) eaav0693.
- [48] B.K. Banerjee, On a generalised approach to first and second order magnetic transitions, *Phys. Lett.* 12 (1964) 16–17.
- [49] J.A. Barclay, W.A. Steyert, Materials for magnetic refrigeration between 2K and 20K, *Cryogenics* 22 (1982) 73–80.
- [50] L.D. Griffith, Y. Mudryk, J. Slaughter, V.K. Pecharsky, Material-based figure of merit for caloric materials, *J. Appl. Phys.* 123 (2018) 034902.
- [51] L.W. Li, Y. Yuan, Y. Zhang, T. Namiki, K. Nishimura, R. Pöttgen, S. Zhou, Giant low field magnetocaloric effect and field-induced metamagnetic transition in TmZn , *Appl. Phys. Lett.* 107 (2015) 132401.
- [52] L.W. Li, K. Nishimura, W.D. Hutchison, Z. Qian, D. Huo, T. NamiKi, Giant reversible magnetocaloric effect in ErMn_2Si_2 compound with a second order magnetic phase transition, *Appl. Phys. Lett.* 100 (2012) 152403.
- [53] M. Das, S. Roy, N. Khan, P. Mandal, Giant magnetocaloric effect in an exchange-frustrated GdCrTiO_5 antiferromagnet, *Phys. Rev. B* 98 (2018) 104420.
- [54] W. Liu, F. Liang, Y. Chen, H. Song, J. Feng, J. Shen, Z. Lin, H. Tu, G. Zhang, Large magnetocaloric effect in $\text{Li}_3\text{K}_9\text{Gd}_3(\text{BO}_3)_7$ crystal featuring sandwich-like three-dimensional framework, *Inorg. Chem.* 60 (2021) 6796–6803.
- [55] S. Roy, N. Khan, P. Mandal, Giant low-field magnetocaloric effect in single-crystalline $\text{EuTi}_{0.85}\text{Nb}_{0.15}\text{O}_3$, *APL Mater.* 4 (2016) 026102.
- [56] S. Mahana, U. Manju, D. Topwal, GdCrO_3 : a potential candidate for low temperature magnetic refrigeration, *J. Phys. D Appl. Phys.* 51 (2018) 305002.
- [57] M. Das, S. Roy, P. Mandal, Giant reversible magnetocaloric effect in a multiferroic GdFeO_3 single crystal, *Phys. Rev. B* 96 (2017) 174405.
- [58] V. Franco, A. Conde, J.M.R. Enrique, J.S. Blázquez, A universal curve for the magnetocaloric effect: an analysis based on scaling relations, *J. Phys. Condens. Matter* 20 (2008) 285207.
- [59] V. Franco, A. Conde, Scaling laws for the magnetocaloric effect in second order phase transitions: from physics to applications for the characterization of materials, *Int. J. Refrig.* 33 (2010) 465–473.
- [60] D. Guo, L.M. Moreno-Ramírez, C. Romero-Muñiz, Y. Zhang, J.Y. Law, V. Franco, J. Wang, Z. Ren, First- and second-order phase transitions in $\text{RE}_6\text{Co}_2\text{Ga}$ ($\text{RE} = \text{Ho}, \text{Dy}$ or Gd) cryogenic magnetocaloric materials, *Sci. China Mater.* 64 (2021) 2846–2857.
- [61] L.M. Moreno-Ramírez, J.Y. Law, S.S. Pramana, A.K. Giri, V. Franco, Analysis of the magnetic field dependence of the isothermal entropy change of inverse magnetocaloric materials, *Res. Phys.* 22 (2021) 103933.
- [62] J.Y. Law, V. Franco, L.M. Moreno-Ramírez, A. Conde, D.Y. Karpenkov, I. Radulov, K.P. Skokov, O. Gutfleisch, A quantitative criterion for determining the order of magnetic phase transitions using the magnetocaloric effect, *Nat. Commun.* 9 (2018) 2680.